Applied Mathematics and Computation 329 (2018) 23–37

Contents lists available at ScienceDirect

Applied Mathematics and Computation

journal homepage: www.elsevier.com/locate/amc

High order well-balanced discontinuous Galerkin methods for Euler equations at isentropic equilibrium state under gravitational fields

Shouguo Qian[a], Yu Liu[a], Gang Li[a,*], Li Yuan[b]

[a] School of Mathematics and Statistics, Qingdao University, Qingdao, Shandong 266071, PR China
[b] LSEC & NCMIS, Institute of Computational Mathematics and Scientific/Engineering Computing, Academy of Mathematics and Systems Science, Chinese Academy of Sciences, Beijing 100190, PR China

ARTICLE INFO

Keywords:
Euler equations
Isentropic equilibrium state
Discontinuous Galerkin methods
Well-balanced property
Gravitational fields

ABSTRACT

Euler equations under gravitational fields often appear in some interesting astrophysical and atmospheric applications. The Euler equations are coupled with gravitational source term due to the gravity and admit hydrostatic equilibrium state where the flux produced by the pressure gradient is exactly balanced by the gravitational source term. In this paper, we construct high order discontinuous Galerkin methods for the Euler equations under gravitational fields, which are well-balanced for the isentropic type hydrostatic equilibrium state. To maintain the well-balanced property, we first reformulate the governing equations in an equivalent form. Then we propose a novel source term approximation based on a splitting algorithm as well as well-balanced numerical fluxes. Rigorous theoretical analysis and extensive numerical examples all suggest that the proposed methods maintain the hydrostatic equilibrium state up to the machine precision. Moreover, one- and two-dimensional simulations are performed to test the ability of the current methods to capture small perturbation of such equilibrium state, and the genuine high order accuracy in smooth regions.

1. Introduction

Hydrodynamical evolution under gravitational fields frequently arises in many applications [1,2] including the astrophysics and the numerical weather prediction. Specific examples include the researches of atmospheric phenomena that are intrinsical in numerical weather prediction and in climate modelling. In addition, there are a wide variety of studies in astrophysics for instance modelling solar climate and simulating supernova explosions. In general, the hydrodynamical evolution can be modeled by the compressible Euler equations coupled with a gravitational source term:

$$\begin{aligned} &\rho_t + \nabla \cdot (\rho \mathbf{u}) = 0, \\ &(\rho \mathbf{u})_t + \nabla \cdot (\rho \mathbf{u} \otimes \mathbf{u} + p \mathbf{I}_d) = -\rho \nabla \phi, \\ &E_t + \nabla \cdot ((E + p)\mathbf{u}) = -\rho \mathbf{u} \cdot \nabla \phi, \end{aligned} \tag{1}$$

* Corresponding author.
E-mail address: gangli1978@163.com (G. Li).

https://doi.org/10.1016/j.amc.2018.01.059
0096-3003/

where $\mathbf{x} \in \mathcal{R}^d$ $(d = 1, 2, 3)$ is the spatial variable, ρ denotes the fluid density, $\mathbf{u}$ is the velocity, p represents the pressure, and $E = \frac{1}{2}\rho\|\mathbf{u}\|^2 + \rho e$ (e is internal energy) is the non-gravitational total energy which includes the kinetic and internal energy of the fluid. $\phi = \phi(\mathbf{x})$ is the time independent gravitational potential. The operators ∇, $\nabla\cdot$ and $\otimes$ are the gradient, divergence and tensor product in $\mathcal{R}^d$, respectively, and $\mathbf{I}_d$ stands for the identity matrix. To close the system, the pressure p is linked to the density and the internal energy through an equation of state denoted by

$$p = (\gamma - 1)\rho e = (\gamma - 1)\big(E - \rho\|\mathbf{u}\|^2/2\big), \tag{2}$$

with γ being the ratio of specific heats.

The system (1) belongs to hyperbolic balance laws and admits steady state solutions (also called as hydrostatic equilibrium state), in which the source term is exactly balanced by the non-zero flux gradient. Specifically speaking, there are two well-known hydrostatic equilibriums states, i.e., the isothermal [3] and the isentropic equilibrium state [2], which will be explained in detail in Section 2. Many practical problems [2–9] involve nearly steady state flows under gravitational fields, therefore it is essential to correctly capture the effect of gravitational force in these simulations, especially if a long-time integration is involved, for example in the modeling galaxy formation [2] and in the atmosphere modeling [9]. However,the standard numerical methods generally fail to maintain the steady state exactly, and result in spurious numerical oscillations even with much refined mesh [10]. Greenberg et al. [11,12] in 1997 originally introduced well-balanced methods, which preserve exactly the steady state solutions up to the machine precision. In addition, compared with the non-well-balanced ones, the well-balanced methods can accurately resolve small perturbations of such steady state with relatively coarse meshes [10,13].

In recent years, well-balanced methods have attracted much attention. LeVeque and Bale [14] extended the quasi-steady wave-propagation methods to the Euler equations under a static gravitational fields. Finite volume well-balanced discretizations with respect to dominant hydrostatics have been proposed by Botta et al. [9] for the nearly hydrostatic flows in the numerical weather prediction. Xu and his collaborators [4–6] have extended the gas-kinetic scheme to the multidimensional gas dynamic equations. Käppeli and Mishra [2] have proposed well-balanced finite volume schemes for the isentropic hydrostatic equilibrium. High order well-balanced finite difference weighted essentially non-oscillatory (WENO) schemes for the isothermal equilibrium are introduced in [3,15] by means of the reformulation of the governing equations. The first attempt of discontinuous Galerkin (DG) methods the isothermal model has been conducted by Li and Xing [16] based on the technique in [3]. Recently, Li and Xing designed high order well-balanced finite volume WENO schemes for both isothermal and isentropic models [17]. More recently, Li and Xing developed high order well-balanced finite difference WENO schemes [18] and well-balanced DG methods [19] for the isentropic models. Well-balanced finite volume schemes for the general hydrostatic equilibrium without any assumption of a thermal equilibrium are recently studied in [1,2,8]. Other related work on well-balanced methods can be found in [20–23].

The main objective of this study is to develop high order well-balanced DG methods for the Euler equations at isentropic equilibrium state under gravitational fields. DG methods are a class of finite element methods using discontinuous piecewise polynomial space as the solution and test function spaces (see [24,25] for a brief historic review). Several advantages of the DG method, including its accuracy, easy implementation of parallel computing, flexibility for hp-adaptation, convenient treatment for the boundary conditions and arbitrary geometry and meshes, make it useful for a wide range of applications [26–28].

Herein, in order to achieve well-balanced property, we first reformulate the source term in an equivalent form by means of the hydrostatic equilibrium state. Then, we propose well-balanced numerical fluxes as well as a novel source term approximation. Ultimately, the high order numerical approximations to the fluxes gradient are exactly balanced with those to the gravitational source term for the isentropic equilibrium state.

This paper is organized as follows. In Section 2, we present well-balanced DG methods for the one-dimensional problems. Subsequently, we extend the proposed well-balanced methods to multi-dimensional problems in Section 3. Section 4 contains extensive one- and two-dimensional numerical results to demonstrate the performance of proposed DG methods. Some conclusions are given in Section 5.

2. Well-balanced DG methods for one-dimensional cases

In this section, we first present the mathematical model of one-dimensional cases as well as hydrostatic equilibrium states. Subsequently, we construct well-balanced DG methods.

2.1. The mathematical model

In one spatial dimension, the model takes the following form

$$\begin{aligned} &\rho_t + (\rho u)_x = 0, \\ &(\rho u)_t + (\rho u^2 + p)_x = -\rho\phi_x, \\ &E_t + ((E + p)u)_x = -\rho u\phi_x. \end{aligned} \tag{3}$$

There exists the hydrostatic equilibrium state, where the gravitational force is exactly balanced by the pressure gradient force:

$$u = 0, \quad p_x = -\rho\phi_x. \tag{4}$$

However, only with the relation (4) at hand, the pressure stratifications are not uniquely defined due to [2]. In general, one must specify the profile of the temperature or the entropy, to determine the stable equilibrium. Accordingly, two important special equilibrium, i.e., the isothermal (constant temperature) [3] and isentropic (constant entropy) hydrostatic equilibrium states [2], arise in the applications.

For an ideal gas satisfying

$$p(x) = \rho(x)RT(x), \tag{5}$$

with R being the gas constant, we can integrate the steady state solutions (4) and obtain

$$\rho = \frac{p_0}{RT(x)}\exp\left(-\int_{x_0}^{x}\frac{\phi_x(s)}{RT(s)}\mathrm{d}s\right), \qquad u = 0, \qquad p = p_0\exp\left(-\int_{x_0}^{x}\frac{\phi_x(s)}{RT(s)}\mathrm{d}s\right), \tag{6}$$

where p_0 is the initial pressure at some reference position x_0.

For the isothermal equilibrium state, the temperature $T(x)\equiv T_0$ becomes a constant, and the equilibrium correspondingly becomes

$$\rho = \rho_0\exp\left(-\frac{\phi}{RT_0}\right), \qquad u = 0, \qquad p = p_0\exp\left(-\frac{\phi}{RT_0}\right), \tag{7}$$

with $p_0 = \rho_0 RT_0$.

The other isentropic hydrostatic equilibrium is usually characterized by Käppeli and Mishra [8]

$$p = K\rho^{\gamma}, \tag{8}$$

which will lead to the form of

$$\rho = \left(\frac{\gamma-1}{K\gamma}(C-\phi)\right)^{\frac{1}{\gamma-1}}, \qquad u = 0, \qquad p = \frac{1}{K^{\frac{1}{\gamma-1}}}\left(\frac{\gamma-1}{\gamma}(C-\phi)\right)^{\frac{\gamma}{\gamma-1}}, \tag{9}$$

where C and K are both constants and γ is the ratio of specific heats in (2). As shown in [2], an equivalent formulation of (9) is given by

$$u = 0, \quad h + \phi = C, \tag{10}$$

where $h = e + \frac{p}{\rho}$ denotes the specific enthalpy. In fact, the equilibrium (10) is obtained from the thermodynamics relation $\mathrm{d}h = T\mathrm{d}s + \frac{1}{\rho}\mathrm{d}p$. In the case of constant entropy, we have $\mathrm{d}s\equiv 0$, which leads to $\mathrm{d}h = \frac{1}{\rho}\mathrm{d}p = -\mathrm{d}\phi$, namely $\mathrm{d}(h+\phi) = 0$, which consequently results in (10). Consequently, we rewrite isentropic equilibrium state (9) can also be rewritten as follows

$$\rho = \left(\frac{\gamma-1}{K\gamma}h\right)^{\frac{1}{\gamma-1}}, \qquad u = 0, \qquad p = \frac{1}{K^{\frac{1}{\gamma-1}}}\left(\frac{\gamma-1}{\gamma}h\right)^{\frac{\gamma}{\gamma-1}}, \tag{11}$$

based on $\phi = C - h$ from (10). In this study, we only consider the isentropic equilibrium state (11).

2.2. One-dimensional DG methods

2.2.1. Notations

We begin with presenting some standard notations under the framework of DG methods. Firstly, we divide the interval $I = [a, b]$ into N subintervals and denote the cells by $I_j = [x_{j-\frac{1}{2}}, x_{j+\frac{1}{2}}]$ for $j = 1, \ldots, N$. The center of each cell is $x_j = \frac{1}{2}(x_{j-\frac{1}{2}} + x_{j+\frac{1}{2}})$, and the mesh size is denoted by $h_j = x_{j+\frac{1}{2}} - x_{j-\frac{1}{2}}$, with $h = \max\limits_{1\le j\le N} h_j$ being the maximal mesh size. The following piecewise polynomial space

$$V_h^k = \left\{v : v|_{I_j} \in P^k(I_j),\ j = 1, 2, \ldots, N\right\}. \tag{12}$$

is defined as the space of polynomials of degree up to k in each cell I_j. Note that the functions in V_h^k are allowed to have discontinuities across the element interfaces.

For any unknown u, its numerical approximation in the DG methods is denoted by u_h, which belongs to the finite element space V_h^k. We denote by $u^+_{h,j+\frac{1}{2}}$ and $u^-_{h,j+\frac{1}{2}}$ the limit values of u_h at $x_{j+\frac{1}{2}}$ from the right cell I_{j+1} and from the left cell I_j, respectively. The usual notation

$$\{u_h\} = \frac{1}{2}(u_h^+ + u_h^-) \tag{13}$$

is applied to represent the arithmetic average of the function u_h at the element interfaces.

2.2.2. Reformulation of the governing equations

The general steady state solutions are given by (4), and we would like to design well-balanced DG methods which preserve such steady states which satisfy the following assumption:

The targeting isentropic equilibrium state to be preserved in the form of (4) are explicitly known and can be denoted by means of $\rho^e(x)$ and $p^e(x)$ (or $\rho^e(x)$ and $E^e(x)$).

Therefore, (4) leads to the following fact

$$p^e(x)_x = -\rho^e(x)\phi_x. \tag{14}$$

In order to construct well-balanced methods, based on (14) and follow the idea of [3], we firstly write the source term in the form as follows

$$-\rho\phi_x = \frac{\rho}{\rho^e}p^e_x$$

with the help of (14). Subsequently, we reformulate the original governing Eq. (3) into the following form

$$\begin{aligned}
&\rho_t + (\rho u)_x = 0\\
&(\rho u)_t + \left(\rho u^2 + p\right)_x = \frac{\rho}{\rho^e}p^e_x\\
&E_t + ((E+p)u)_x = -\rho u\phi_x,
\end{aligned} \tag{15}$$

with $\rho^e = \left(\frac{\gamma-1}{K\gamma}(C-\phi)\right)^{\frac{1}{\gamma-1}}$ and $p^e = \frac{1}{K^{\frac{1}{\gamma-1}}}\left(\frac{\gamma-1}{\gamma}(C-\phi)\right)^{\frac{\gamma}{\gamma-1}}$ being the density and pressure at the isentropic equilibrium state due to (11). As a consequence, this system can be written in a compact vector form

$$U_t + F(U)_x = S,$$

with U, $F(U)$ and S being the unknown vector, the flux and the source term, respectively.

Under the framework of the DG methods, we denote the DG approximation to the solution U by $U_h \in V_h^k$. The semi-discrete DG methods for (15) are defined as follows: for any test function $v \in V_h^k$, U_h is given by

$$\int_{I_j}(U_h)_t v\mathrm{d}x - \int_{I_j}F(U_h)v_x\mathrm{d}x + \widehat{F}_{j+\frac{1}{2}}v(x^-_{j+\frac{1}{2}}) - \widehat{F}_{j-\frac{1}{2}}v(x^+_{j-\frac{1}{2}}) = \int_{I_j}Sv\mathrm{d}x, \tag{16}$$

with $\widehat{F}_{j+\frac{1}{2}} = f\left(U^-_{h,j+\frac{1}{2}},\ U^+_{h,j+\frac{1}{2}}\right)$ being the numerical flux. Herein, we adopt $f(a, b)$ as a numerical flux. One example is the simple Lax–Friedrichs flux

$$f(a,b) = \frac{1}{2}(F(a) + F(b) - \alpha(b-a)), \tag{17}$$

where $\alpha = \max_x \left|\lambda(U)\right|$ with $\lambda(U)$ being the eigenvalues of the Jacobian matrix $F'(U)$, and the maximum is taken over the whole region.

2.2.3. Novel source term approximation

The semi-discrete well-balanced DG methods still take the form of (16), but with modified numerical fluxes and the source term approximations outlined below. Firstly, based on a splitting algorithm, we decompose the integral of the source term in the second equation as follows

$$\begin{aligned}
\int_{I_j}S^{[2]}v\,\mathrm{d}x &= \int_{I_j}\frac{\rho}{\rho^e}p^e_x v\,\mathrm{d}x\\
&= \int_{I_j}\left(\frac{\rho}{\rho^e} - \frac{\rho(x_j)}{\rho^e(x_j)} + \frac{\rho(x_j)}{\rho^e(x_j)}\right)p^e_x v\,\mathrm{d}x\\
&= \int_{I_j}\left(\frac{\rho}{\rho^e} - \frac{\rho(x_j)}{\rho^e(x_j)}\right)p^e_x v\,\mathrm{d}x + \frac{\rho(x_j)}{\rho^e(x_j)}\int_{I_j}p^e_x v\,\mathrm{d}x\\
&= \int_{I_j}\left(\frac{\rho}{\rho^e} - \frac{\rho(x_j)}{\rho^e(x_j)}\right)p^e_x v\,\mathrm{d}x\\
&\quad + \frac{\rho(x_j)}{\rho^e(x_j)}\left(p^e_{h,j+\frac{1}{2}}v(x^-_{j+\frac{1}{2}}) - p^e_{h,j-\frac{1}{2}}v(x^+_{j-\frac{1}{2}})\right) - \frac{\rho(x_j)}{\rho^e(x_j)}\int_{I_j}p^e v_x\,\mathrm{d}x,
\end{aligned} \tag{18}$$

where the last line of the above equality is due to the integration by parts for the integral $\frac{\rho(x_j)}{\rho^e(x_j)}\int_{I_j}p^e_x v\,\mathrm{d}x$. Subsequently, we

approximate (18) by

$$\int_{I_j} S^{[2]} v \,\mathrm{d}x \approx \int_{I_j} \left(\frac{\rho}{\rho^e} - \frac{\rho(x_j)}{\rho^e(x_j)}\right) p^e_x v \,\mathrm{d}x + \frac{\rho(x_j)}{\rho^e(x_j)} \left(\left\{ p^e_{h,j+\frac{1}{2}} \right\} v(x^-_{j+\frac{1}{2}}) - \left\{ p^e_{h,j-\frac{1}{2}} \right\} v(x^+_{j-\frac{1}{2}}) \right) - \frac{\rho(x_j)}{\rho^e(x_j)} \int_{I_j} p^e v_x \,\mathrm{d}x, \tag{19}$$

where $p^e_{h,j\pm\frac{1}{2}}$ are replaced by $\left\{ p^e_{h,j\pm\frac{1}{2}} \right\} = \frac{1}{2}\left(p^{e,-}_{h,j\pm\frac{1}{2}} + p^{e,+}_{h,j\pm\frac{1}{2}} \right)$ as in (13). The integral of the source term in the third equation can be approximated by suitable Gaussian quadrature rule.

Remark 1. The main purpose of the splitting in Eq. (18) is to balance the source term approximation and the approximation to the flux gradient, which will be validated in the proof of the following Proposition 1 in Section 2.2.5. In fact, a straightforward approximation to the source term $\int_{I_j} S^{[2]} v \,\mathrm{d}x$ does not lead to well-balanced methods correspondingly.

2.2.4. Well-balanced numerical fluxes

The last step in designing well-balanced DG methods is to construct the numerical fluxes $\widehat{F}_{j+\frac{1}{2}}$. The term $\alpha(b-a)$ in the Lax–Friedrichs flux (17) contributes to the numerical viscosity term, which is essential for the nonlinear hyperbolic conservation laws. However, here they will destroy the well-balanced property for the equilibrium state. So, we apply a flux modification technique to construct the numerical flux in the following form

$$\widehat{F}_{j+\frac{1}{2}} = \frac{1}{2}\left[F\left(U^-_{h,j+\frac{1}{2}}\right) + F\left(U^+_{h,j+\frac{1}{2}}\right) - \widetilde{\alpha}\left(\widetilde{U}^+_{h,j+\frac{1}{2}} - \widetilde{U}^-_{h,j+\frac{1}{2}}\right)\right], \tag{20}$$

with the coefficient $\widetilde{\alpha}$ being defined as

$$\widetilde{\alpha} = \alpha \max_j \left(\rho^e_j,\ p^e_j\right), \tag{21}$$

and $\widetilde{U}$ is given by

$$\widetilde{U} = \left(\frac{\rho}{\rho^e(x)}, \frac{\rho u}{\rho^e(x)}, \frac{E}{p^e(x)}\right)^T,$$

It is obvious that $\widetilde{U} = constant$ at the isentropic equilibrium state and the viscosity terms $\widetilde{\alpha}\left(\widetilde{U}^+_{h,j+\frac{1}{2}} - \widetilde{U}^-_{h,j+\frac{1}{2}}\right)$ become zero accordingly. Therefore, the effect of these viscosity terms disappear. So the numerical flux now reduces correspondingly to the following simple form

$$\widehat{F}_{j+\frac{1}{2}} = \frac{1}{2}\left[F\left(U^-_{h,j+\frac{1}{2}}\right) + F\left(U^+_{h,j+\frac{1}{2}}\right)\right]. \tag{22}$$

2.2.5. Well-balanced methods

All these outlined above lead to well-balanced DG methods for the Euler equations at the isentropic equilibrium state, as presented in the following proposition.

Proposition 1. *For one-dimensional Euler equations (3) under the gravitational fields, the semi-discrete DG methods (16), combined with (19) and (20), are well-balanced for the isentropic equilibrium state (4).*

Proof. At the isentropic equilibrium state (11), it is obvious to observe that the well-balanced property holds for the first and the third equations, as both the numerical flux and source term approximation in these equations become zero due to $u = 0$. For the second equation, the source term approximation becomes

$$\int_{I_j} S^{[2]} v \,\mathrm{d}x \approx \frac{\rho(x_j)}{\rho^e(x_j)} \left(\left\{ p^e_{h,j+\frac{1}{2}} \right\} v(x^-_{j+\frac{1}{2}}) - \left\{ p^e_{h,j-\frac{1}{2}} \right\} v(x^+_{j-\frac{1}{2}}) \right) - \frac{\rho(x_j)}{\rho^e(x_j)} \int_{I_j} p^e v_x \,\mathrm{d}x. \tag{23}$$

In addition, since $u = 0$, so the second flux term $F^{[2]} = \rho u^2 + p$ reduces to p, and its numerical approximation takes the following form:

$$\widehat{F}^{[2]}_{j+\frac{1}{2}} v(x^-_{j+\frac{1}{2}}) - \widehat{F}^{[2]}_{j-\frac{1}{2}} v(x^+_{j-\frac{1}{2}}) - \int_{I_j} p v_x \,\mathrm{d}x = \left(\left\{ p_{h,j+\frac{1}{2}} \right\} v(x^-_{j+\frac{1}{2}}) - \left\{ p_{h,j-\frac{1}{2}} \right\} v(x^+_{j-\frac{1}{2}}) \right) - \int_{I_j} p v_x \,\mathrm{d}x. \tag{24}$$

Based on the fact that $\rho = \rho^e$ and $p = p^e$ at the isentropic equilibrium state, we can conclude that the flux and source term approximations balance each other, which indicate that our methods preserve the well-balanced property accordingly. Finally, we finish the proof. □

For the temporal discretization, we apply the third order total variation diminishing (TVD) Runge–Kutta methods [29]:

$$\begin{aligned} U^{(1)} &= U^n + \Delta t \mathcal{F}(U^n) \\ U^{(2)} &= \frac{3}{4}U^n + \frac{1}{4}\left(U^{(1)} + \Delta t \mathcal{F}(U^{(1)})\right) \\ U^{n+1} &= \frac{1}{3}U^n + \frac{2}{3}\left(U^{(2)} + \Delta t \mathcal{F}(U^{(2)})\right), \end{aligned} \tag{25}$$

with $\mathcal{F}(U)$ being the spatial operator.

Subsequently, we summarize the complete algorithm of the current high order DG methods for the one-dimensional Euler equations (3) at isentropic equilibrium state (4):

1. Firstly, to reformulate the source term and rewrite the governing equations in the form (15).
2. At each time step, apply a flux modification technique to construct the numerical flux as in (20).
3. Evaluate the source term with a novel source term approximation (19) at the current time step.
4. Add up the residues of the numerical flux and source term approximations and obtain a semi-discrete DG methods (16), then forward in time by the third order Runge–Kutta methods (25).

In the end, a slope limiter procedure is usually needed for the occasions with discontinuous solutions. In general, the implementation of a slope limiter on the unknown U_h involves two steps. The first step is to check whether any limiting is necessary in cell I_j based on the cell averages $(\overline{U}_h)_j$, $(\overline{U}_h)_{j\pm1}$ as well as $U^+_{h,j-\frac{1}{2}}$ and $U^-_{h,j+\frac{1}{2}}$. If the answer is positive, the second step is to apply the given slope limiter on the variables U_h in the cell I_j. In this study, we employ the total variation bounded (TVB) limiter presented in [30,31].

3. Extension to multi-dimensional cases

In this section, we present well-balanced DG methods to multi-dimensional cases on structured meshes. The multi-dimensional isentropic equilibrium state we are interested to preserve takes the form of

$$\rho = \left(\frac{\gamma-1}{K\gamma}(C-\phi)\right)^{\frac{1}{\gamma-1}}, \qquad \mathbf{u} = 0, \qquad p = \frac{1}{K^{\frac{1}{\gamma-1}}}\left(\frac{\gamma-1}{\gamma}(C-\phi)\right)^{\frac{\gamma}{\gamma-1}}. \tag{26}$$

Let $\mathcal{T}_\tau$ be a family of partitions of the computational domain Ω parameterized by $\tau > 0$. We do not specify the mesh element here. For multi-dimensional cases, well-balanced DG methods proposed below work for both rectangular and triangular meshes. For any element $K \in \mathcal{T}_\tau$, we define $\tau_K := \mathrm{diam}(K)$ and $\tau := \max_{K\in\mathcal{T}_\tau} \tau_K$. For each edge e^i_K $(i = 1, \ldots, m)$ of K, we denote the outward unit normal vector by ν^i_K and the area of the element K by $|K|$.

Firstly, we rewrite the multi-dimensional Euler equations (1) by

$$\mathbf{U}_t + \nabla \cdot \mathbf{F}(U) = S,$$

where $\mathbf{U} = (\rho, \rho\mathbf{u}, E)^T$, $\mathbf{F}(\mathbf{U})$ denotes the flux and $S = \left(0, \frac{\rho}{\rho^e}\nabla p^e, -\rho\mathbf{u}\cdot\nabla\phi\right)^T$ is the source term. The DG approximation $\mathbf{U}_h$ belongs to the finite dimensional polynomial space

$$V^k_\tau \equiv \{w \in L^2(\Omega) : \ w|_K \in P^k(K), \ \forall\, K \in \mathcal{T}_\tau\}, \tag{27}$$

where $P^k(K)$ denotes the space of polynomials on the element K with at most kth degree. The semi-discrete DG method is given by

$$\int_K \partial_t \mathbf{U} w \,\mathrm{d}\mathbf{x} - \int_K \mathbf{F}(\mathbf{U})\cdot\nabla w \,\mathrm{d}\mathbf{x} + \sum_{i=1}^m \int_{e^i_K} \widehat{\mathbf{F}}|_{e^i_K}\cdot\nu^i_K w \,\mathrm{d}s = \int_K S w \,\mathrm{d}\mathbf{x}, \tag{28}$$

where $w(\mathbf{x}) \in V^k_\tau$ is a test function. The numerical flux $\widehat{\mathbf{F}}$ is defined by

$$\widehat{\mathbf{F}}|_{e^i_K}\cdot\nu^i_K = \mathcal{F}\left(U_i^{int(K)}, U_i^{ext(K)}, \nu^i_K\right). \tag{29}$$

where $U_i^{int(K)}$ and $U_i^{ext(K)}$ are the approximations to the values on the edge e^i_K obtained from the interior and the exterior of K. The simple global Lax–Friedrichs flux takes the form of

$$\mathcal{F}(a_1, a_2, \nu) = \frac{1}{2}[\mathbf{F}(a_1)\cdot\nu + \mathbf{F}(a_2)\cdot\nu - \alpha(a_2 - a_1)]. \tag{30}$$

We can extend the well-balanced DG methods designed in Section 2.2 to multiple spatial dimensions. The well-balanced approximation to the integral of this source term follows an analogue of the decomposition (18), which leads to

Table 1
L^1 errors and numerical orders of accuracy for the test case of Section 4.1.

	ρ		ρu		E	
N	L^1 error	Order	L^1 error	Order	L^1 error	Order
50	8.23E−03		9.63E−02		9.15E−03	
100	2.30E−03	1.84	2.82E−03	1.77	2.57E−03	1.83
200	4.36E−04	2.40	4.25E−04	2.73	4.12E−04	2.64
400	6.22E−05	2.81	5.73E−05	2.89	5.92E−05	2.80
800	7.99E−06	2.96	7.06E−06	3.02	7.82E−06	2.92
1600	9.92E−07	3.01	8.95E−07	2.98	9.57E−07	3.03

$$\begin{aligned}\int_K S^{[2]} w\,\mathrm{d}\mathbf{x} &= \int_K \frac{\rho}{\rho^e} p_x^e w\,\mathrm{d}\mathbf{x}\\ &= \int_K \left(\frac{\rho}{\rho^e} - \frac{\rho(\mathbf{x}_K^0)}{\rho^e(\mathbf{x}_K^0)} + \frac{\rho(\mathbf{x}_K^0)}{\rho^e(\mathbf{x}_K^0)}\right) p_x^e w\,\mathrm{d}\mathbf{x}\\ &= \frac{\rho(\mathbf{x}_K^0)}{\rho^e(\mathbf{x}_K^0)}\left(\sum_{i=1}^m \int_{e_k^i} p^e(\mathbf{x}_i^{int(K)})\nu_K^i w\,\mathrm{d}s - \int_K p^e\,\nabla w\,\mathrm{d}\mathbf{x}\right) + \int_K \left(\frac{\rho}{\rho^e} - \frac{\rho(\mathbf{x}_K^0)}{\rho^e(\mathbf{x}_K^0)}\right) p_x^e\, w\,\mathrm{d}\mathbf{x},\end{aligned} \tag{31}$$

where $\mathbf{x}_K^0$ stands for the middle point of the element K. Then, we approximate the source term (31) as follows

$$\int_K S_2 w\,\mathrm{d}\mathbf{x} \approx \frac{\rho(\mathbf{x}_K^0)}{\rho^e(\mathbf{x}_K^0)}\left(\sum_{i=1}^m \int_{e_k^i} \left\{p^e(\mathbf{x}_i^{int(K)})\right\}\nu_K^i w\,\mathrm{d}s - \int_K p^e\,\nabla w\,\mathrm{d}\mathbf{x}\right) + \int_K \left(\frac{\rho}{\rho^e} - \frac{\rho(\mathbf{x}_K^0)}{\rho^e(\mathbf{x}_K^0)}\right) p_x^e\, w\,\mathrm{d}\mathbf{x}, \tag{32}$$

where the boundary values of p^e are replaced by the cell average $\{p^e\}$. In a similar way, we can also discretize the third source term. For the approximation to the remaining equation, we apply the the Gaussian quadrature rule. The last piece in designing the well-balanced DG methods is to replace the Lax–Friedrichs numerical flux (29)–(30) by:

$$\widehat{\mathbf{F}}|_{e_k^i}\cdot\nu_K^i = \frac{1}{2}\left[\mathbf{F}(U_i^{int(K)})\cdot\nu_K^i + \mathbf{F}(U_i^{ext(K)})\cdot\nu_K^i - \alpha'\left(\widetilde{U}_i^{ext(K)} - \widetilde{U}_i^{int(K)}\right)\right], \tag{33}$$

with

$$\widetilde{U} = \left(\frac{\rho}{\rho^e}, \frac{\rho\mathbf{u}}{\rho^e}, \frac{E}{p^e}\right),$$

to maintain enough artificial numerical viscosity. All these together lead to well-balanced DG methods for the multi-dimensional cases, as outlined in the following proposition.

Proposition 2. *For the multi-dimensional Euler equations (1) under the gravitational fields, the semi-discrete DG methods (28), combined with (32) and (33), are well-balanced for the isentropic equilibrium state (26).*

4. Numerical results

In this section, we carry out extensive one- and two-dimensional numerical experiments to demonstrate the performance of the proposed well-balanced DG methods. In all the computations, we apply the third order TVD Runge–Kutta methods (25), coupled with third order finite element DG methods (i.e., $k = 2$). The CFL number is taken as 0.18.

4.1. To test the order of accuracy

We first test the order of accuracy of the present DG methods. In analogy to [1], we take the following initial data

$$\begin{aligned}&\rho(x,0) = \exp(-x),\\ &u(x,0) = 0,\\ &p(x,0) = (1+x)\exp(-x),\end{aligned}$$

coupled with $\phi(x) = x$ as well as $\gamma = 1.4$ on a unit computational domain [0, 1]. Since the exact solutions are not known explicitly, we apply the third order standard DG method for the original system (3) with 12800 cells to obtain reference solutions, and take the reference solutions as the "exact solutions" to compute the numerical errors and the orders. We compute this example up to $t = 0.1$ and demonstrate the numerical errors and the orders of accuracy in Table 1. It is obvious that the present methods keep the third order accuracy.

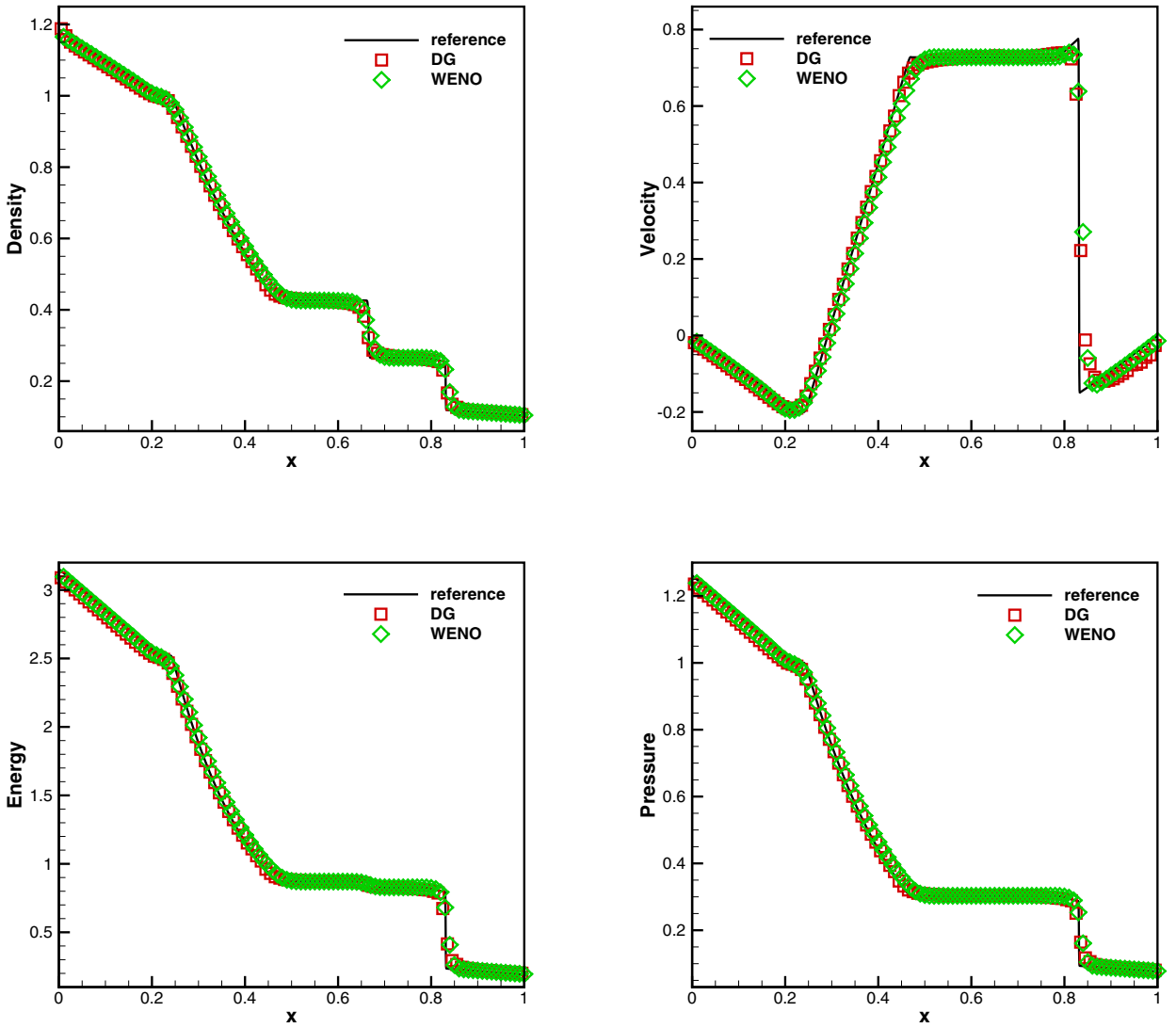

Fig. 1. Shock tube problem under gravitational field in Section 4.2. Numerical results by well-balanced DG methods (denoted by "DG") with 100 cells and by well-balanced WENO schemes (denoted by "WENO") with 100 cells against the reference results at $t = 0.2$. Top left: density; Top right: velocity; Bottom left: energy; Bottom right: pressure.

4.2. One-dimensional shock tube problem under gravitational fields

In this standard Sod test [3], discontinuous initial conditions are given by

$$(\rho, v, p) = \begin{cases} (1, 0, 1) & \text{if } x \le 0.5, \\ (0.125, 0, 0.1) & \text{otherwise}, \end{cases}$$

on a unit computational domain $[0, 1]$ with $\gamma = 1.4$ under a linear gravitational field $g = \phi_x = 1$ acting in the negative x direction.

We present the numerical results at $t = 0.2$ compared with the reference solutions obtained by fifth order well-balanced finite difference WENO schemes [18] with 2000 uniform cells in Fig. 1. For the sake of comparison, we also show the results by the fifth order WENO scheme [18] on a mesh with 200 cells. Due to the presence of the gravitational force, the density distribution is pulling towards the left direction, and negative velocity appears in some regions. By comparing the results in these figures, we can clearly observe that the resulting methods capture sharp discontinuity transition even on a relatively coarse mesh with 100 cells, and agree well with the reference solutions.

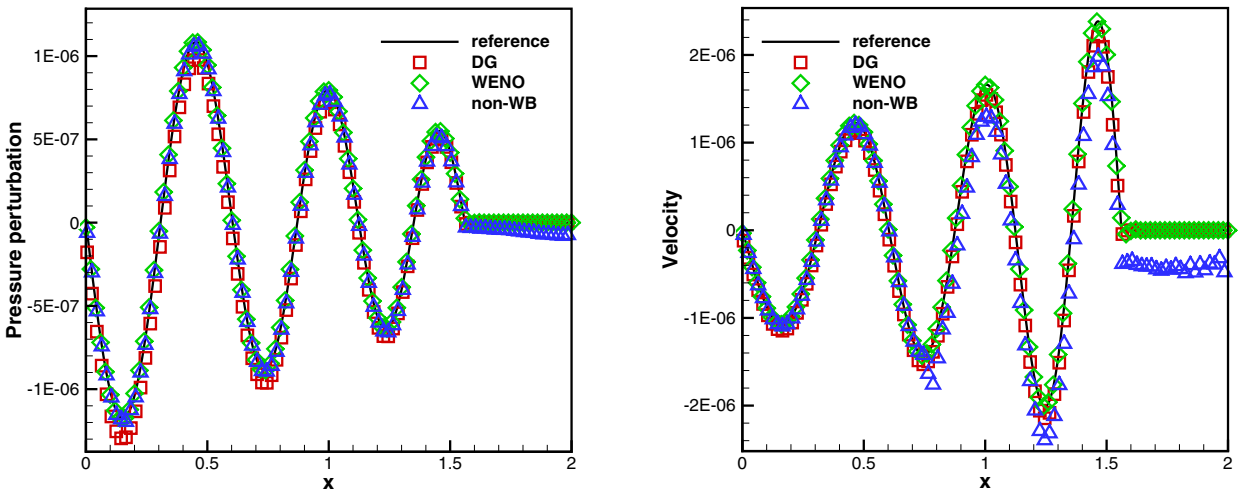

Fig. 2. Small amplitude wave propagation in Section 4.3.2. Numerical results by well-balanced DG methods (denoted by "DG") with 200 cells, by well-balanced WENO schemes (denoted by "WENO") with 200 cells, and by non-well-balanced DG methods (denoted by "non-WB") with 200 cells against the reference results at $t = 0.15$. Pressure perturbation (left) and velocity (right).

Table 2
L^1 errors for different precisions for the steady state solution in Section 4.3.1.

N	Precision	ρ	ρu	E
100	Single	1.74E−6	4.37E−7	3.17E−7
	Double	3.21E−14	4.49E−15	2.37E−15
200	Single	2.25E−6	6.29E−7	7.53E−7
	Double	6.42E−14	6.43E−15	7.57E−15

4.3. Hydrostatic atmosphere in a linear gravitational field

Then we consider a very simple isentropic hydrostatic atmosphere under a linear gravitational field [2]

$$\phi(x) = gx.$$

The steady state data are given by

$$\begin{aligned} \rho(x) &= \left(\rho_0^{\gamma-1} - \frac{1}{K_0}\frac{\gamma-1}{\gamma}gx\right)^{\frac{1}{\gamma-1}}, \\ p(x) &= K_0\rho(x)^{\gamma}, \\ u(x) &= 0, \end{aligned} \tag{34}$$

with $g = 1,\ \gamma = 5/3,\ \rho_0 = 1,\ p_0 = 1$ and $K_0 = p_0/\rho_0^{\gamma}$ on a computational domain $[0, 2]$. In the following, we consider three different test cases, respectively.

4.3.1. Well-balanced property

We consider the first example to test the well-balanced property of the proposed DG methods. The initial conditions are taken as the steady state solutions (34). In order to demonstrate that the steady state is indeed maintained up to the round-off error, we apply single precision and double precision respectively to carry out the computation. We compute this example up to $t = 4$ on meshes with both 100 and 200 uniform cells, and present the L^1 errors of numerical solutions in Table 2. We can clearly observe that the numerical errors are all at the level of round-off error for different precisions, which verify the desired well-balanced property accordingly.

4.3.2. Small amplitude wave propagation

For the second test case, we would to compare the ability of capturing small perturbation on top of the isentropic hydrostatic atmosphere between the well-balanced DG methods and non-well-balanced ones. So we impose a periodic velocity perturbation

$$u(x, t) = A\sin(4\pi t),$$

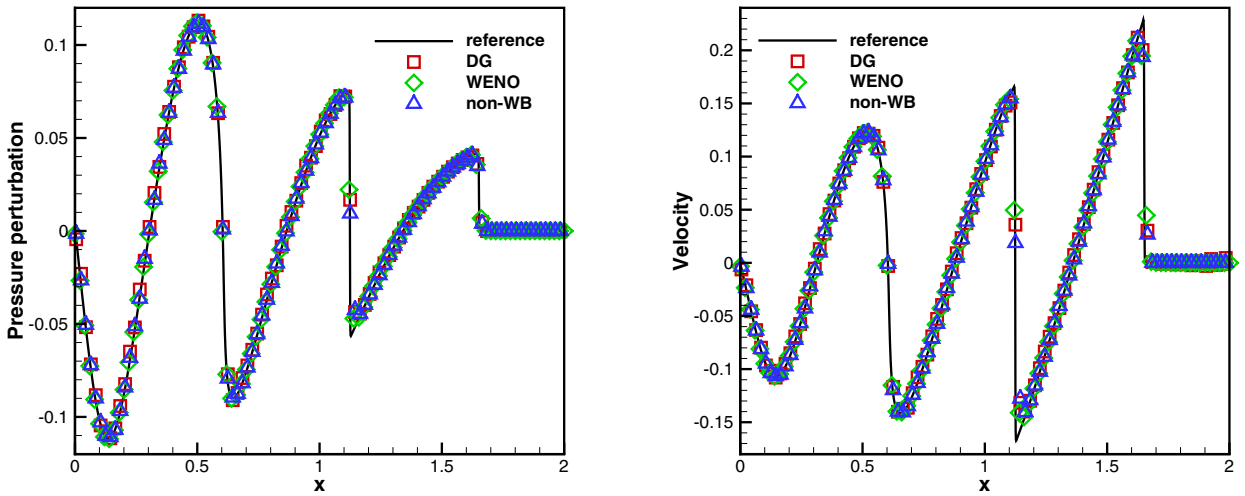

Fig. 3. Large amplitude wave propagation in Section 4.3.3. Numerical results by well-balanced DG methods (denoted by "DG") with 200 cells, by well-balanced WENO schemes (denoted by "WENO") with 200 cells, and by non-well-balanced DG methods (denoted by "non-WB") with 200 cells against the reference results at $t = 0.15$. Pressure perturbation (left) and velocity (right).

at the bottom of the atmosphere. We take $A = 10^{-6}$ for a small amplitude, and compute the generated waves until $t = 1.5$ (shortly before the waves reach the upper boundary). The excited waves move through the whole computational domain and are modified by the density and pressure stratification of the atmosphere.

In Fig. 2, we present the pressure perturbation and the velocity at $t = 1.5$ on a mesh with 200 cells against the reference solutions obtained by the fifth order WENO schemes [18] with 2000 cells. Moreover, we also run the same numerical test by non-well-balanced DG methods with a straightforward integration of the source term, and show their results for the sake of comparison. For the sake of comparison, we also demonstrate the numerical results by the fifth order well-balanced WENO schemes [18] on a mesh with 200 cells. It is obvious that the results by the well-balanced DG methods are in good agreement with the reference solutions. Moreover, Fig. 2 implies that the numerical results produced by different methods are observed to be qualitatively very similar. However, those by the non-well-balanced DG methods are not consistent with the reference solutions for $x > 1.5$. This observation indicates the importance of the well-balanced methods in capturing small amplitude perturbations to the steady state.

4.3.3. Large amplitude wave propagation

For the third test case, we check the robustness of the resulting DG methods even for the large amplitude perturbation with $A = 0.1$. We evolve the generated waves up to $t = 1.5$ (shortly before the waves reach the upper boundary).

Both the numerical results by the well-balanced and non-well-balanced DG methods against the reference solutions (by the fifth order WENO scheme [18] with 2000 cells) are displayed in Fig. 3. In order to make a comparison, we also present the numerical results by the well-balanced WENO schemes [18]. The numerical results by the well-balanced DG methods and WENO schemes [18] continue to keep in line with the reference solutions even for the large amplitude perturbation.

The numerical results of the large amplitude case strongly support that the well-balanced DG methods and WENO schemes can keep the robustness and resolve large perturbation well compared with non-well-balanced one. The above two test cases demonstrates the importance of well-balanced methods in capturing perturbations to the steady states.

4.4. Contact discontinuity under gravitational field

In this test case, we deal with an initial contact discontinuity under a linear gravitational field $\phi(x) = x$ as in [1]. The initial data are defined as follows:

$$(\rho, u, p) = \begin{cases} (1, 0, 1) & \text{if } x < 0.5, \\ (10, 0, 1) & \text{otherwise,} \end{cases}$$

on a computational domain [0, 1] with $\gamma = 1.4$. On both end points, we impose the solid wall boundary conditions. We present the numerical solutions at $t = 0.6$ by well-balanced and non-well-balanced DG methods on a mesh with 200 cells against the reference solutions obtained by the fifth order WENO schemes [18] with 2000 cells in Fig. 4. In addition, we also show the numerical results by the fifth order well-balanced WENO schemes [18] on a mesh with 200 cells and excellent agreement has been evidently achieved. It is obvious that the results by the well-balanced DG methods and WENO schemes are accompanied by high resolution compared with the non-well-balanced one.

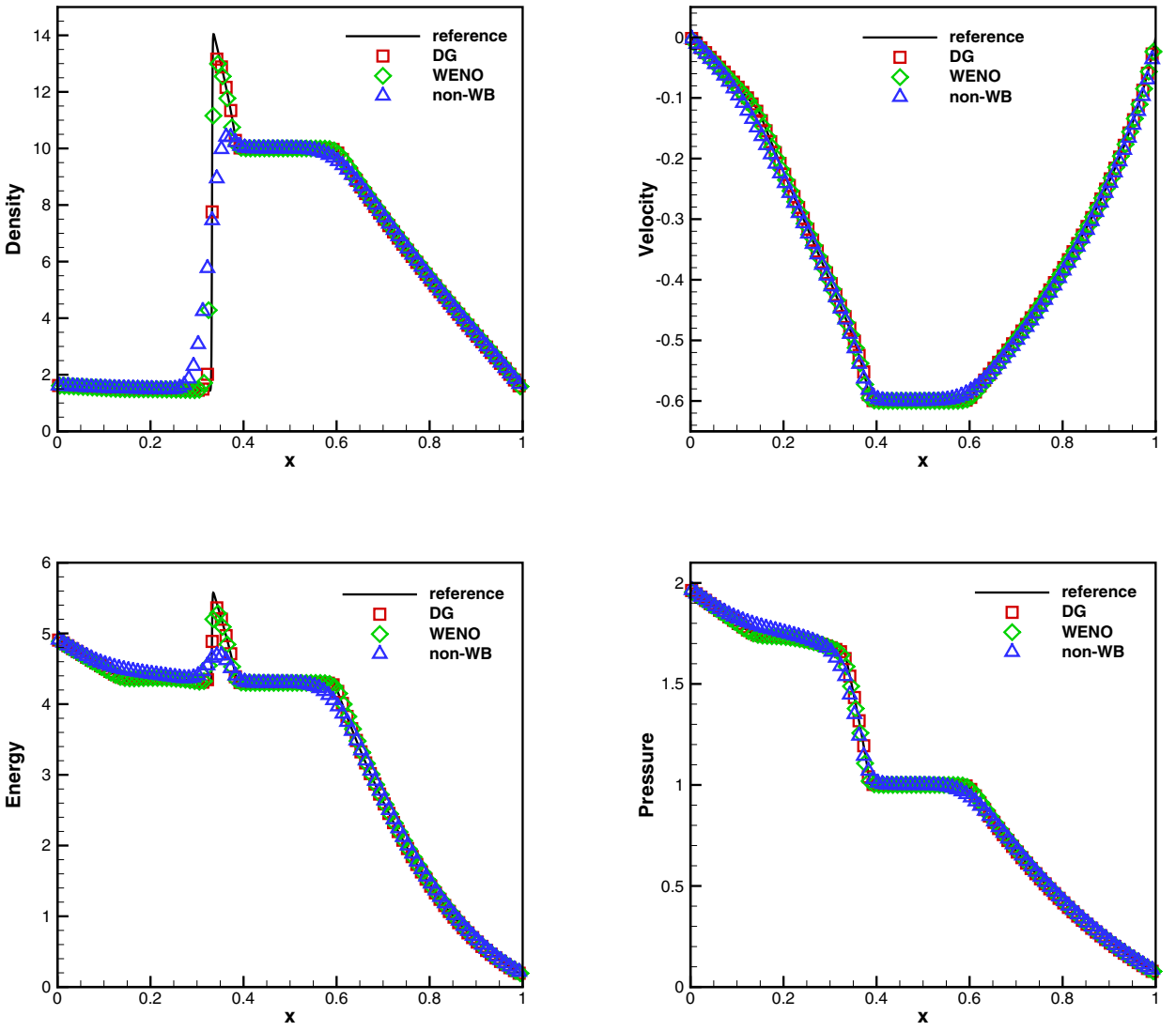

Fig. 4. Contact discontinuity under gravitational field in Section 4.4. Numerical results by well-balanced DG methods (denoted by "DG") with 200 cells, by well-balanced WENO schemes (denoted by "WENO") with 200 cells, and by non-well-balanced DG methods (denoted by "non-WB") with 200 cells against the reference results at $t = 0.6$. Top left: density; Top right: velocity; Bottom left: energy; Bottom right: pressure.

4.5. Two-dimensional polytrope

Subsequently, similar to [2], we consider a two-dimensional test case from the astrophysical problem. These model stars are constructed from the hydrostatic equilibrium:

$$\frac{\mathrm{d}p}{\mathrm{d}r} = -\rho\frac{\mathrm{d}\phi}{\mathrm{d}r}. \tag{35}$$

Herein we will apply $\gamma = 2$, since neutron stars can be modeled by $\gamma \in [2, 3]$. This model has the following steady state

$$\begin{aligned} \rho(r) &= \rho_c \frac{\sin(\alpha r)}{\alpha r}, \\ u(r) &= 0, \\ v(r) &= 0, \\ p(r) &= K\rho(r)^2, \end{aligned} \tag{36}$$

coupled with a given gravitational potential

$$\phi(r) = -2K\rho_c \frac{\sin(\alpha r)}{\alpha r}, \tag{37}$$

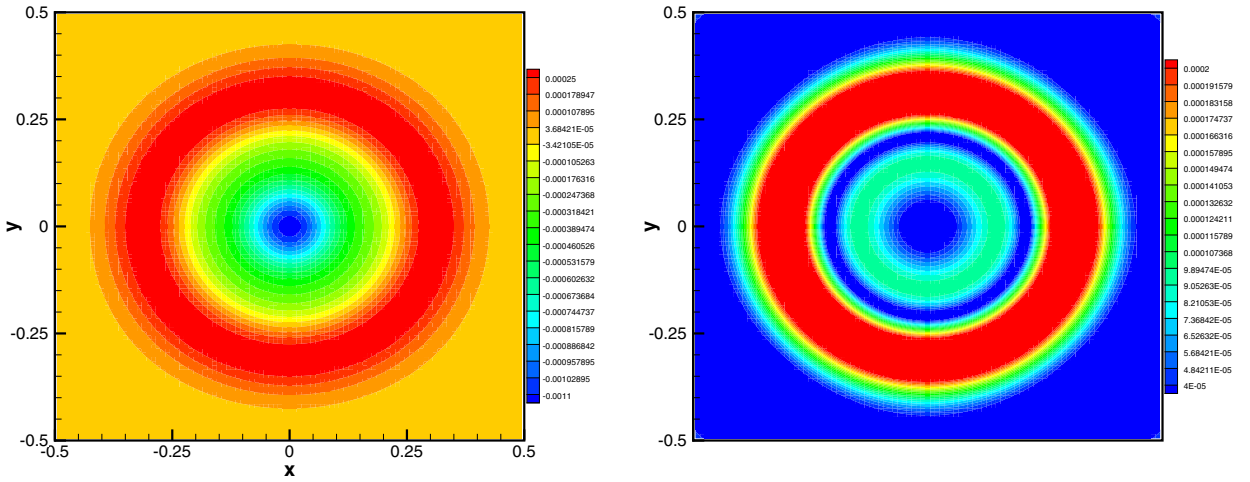

Fig. 5. Two-dimensional polytrope in Section 4.5. Contours of numerical results by well-balanced DG methods with 100×100 cells at $t = 0.2$. Left: pressure perturbation; Right: velocity $\left(\sqrt{u^2 + v^2}\right)$.

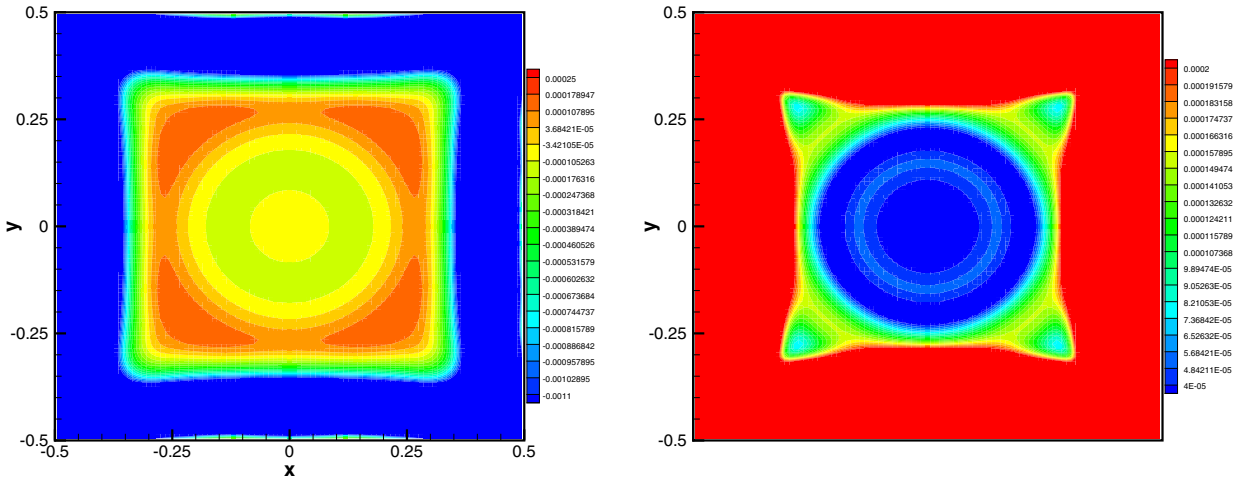

Fig. 6. Two-dimensional polytrope in Section 4.5. Contours of numerical results by non-well-balanced DG methods with 100×100 cells at $t = 0.2$. Left: pressure perturbation; Right: velocity $\left(\sqrt{u^2 + v^2}\right)$.

where $\alpha = \sqrt{\frac{4\pi g}{2K}}$ with $K = g = \rho_c = 1$ and $r = \sqrt{x^2 + y^2}$ being the radial variable. Herein, g represents the gravitational constant.

In order to test the capability of the resulting methods capturing small perturbations of the hydrostatic equilibrium and preserving the axial symmetry at the same time, we initially add a small Gaussian hump perturbations in pressure to the steady state (36) as follows:

$$p(r) = K\rho(r)^2 + 10^{-3}\exp(-100r^2),$$

on a square domain $[-0.5, 0.5] \times [-0.5, 0.5]$.

We evolved the example up to $t = 0.2$ on a mesh with 100×100 uniform cells and present the contour plots of the pressure perturbation and the velocity $\sqrt{u^2 + v^2}$ in Figs. 5 and 6. From these figures, we can clearly observe that the non-well-balanced DG methods are not capable of capturing such small perturbation on the relatively coarse mesh, while the well-balanced ones can resolve it very well. More importantly, the well-balanced DG methods preserve the axial symmetry well, but the non-well-balanced ones fails to keep this symmetry completely.

4.6. Perturbation to the isentropic hydrostatic solution

For the last test case, we consider an isentropic hydrostatic solution inspired by Chandrashekar and Klingenberg [1]

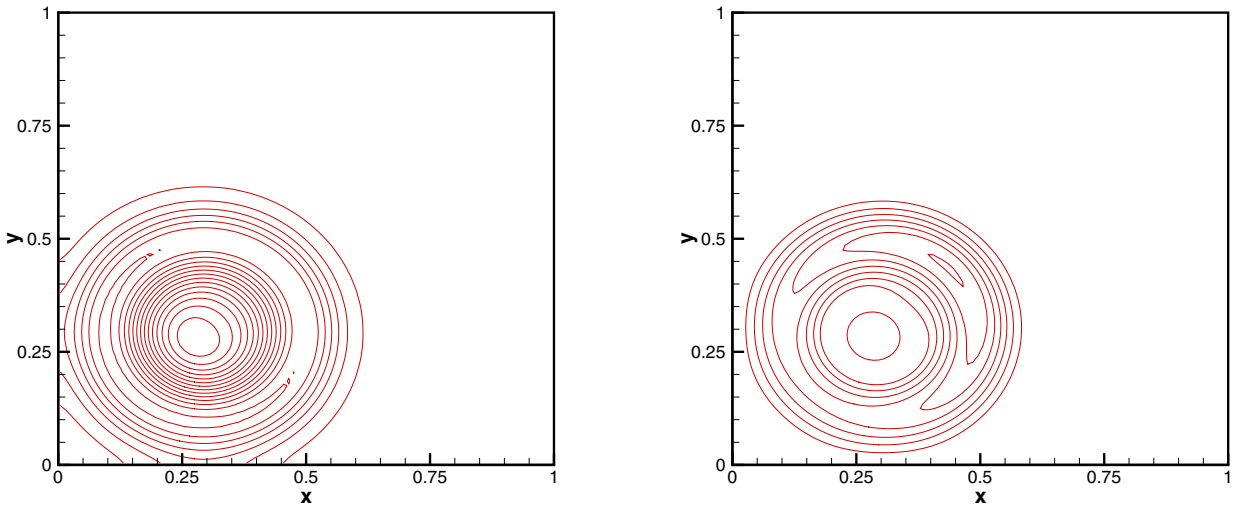

Fig. 7. Perturbation to the polytropic hydrostatic solution with $\eta = 0.1$ in Section 4.6. Contours of numerical results by well-balanced DG methods with 100×100 cells at $t = 0.15$. Left: twenty equally spaced contours between -0.03 and $+0.03$ of pressure perturbation. Right: twenty equally spaced contours between 0.01 and 0.12 of velocity $\left(\sqrt{u^2 + v^2}\right)$.

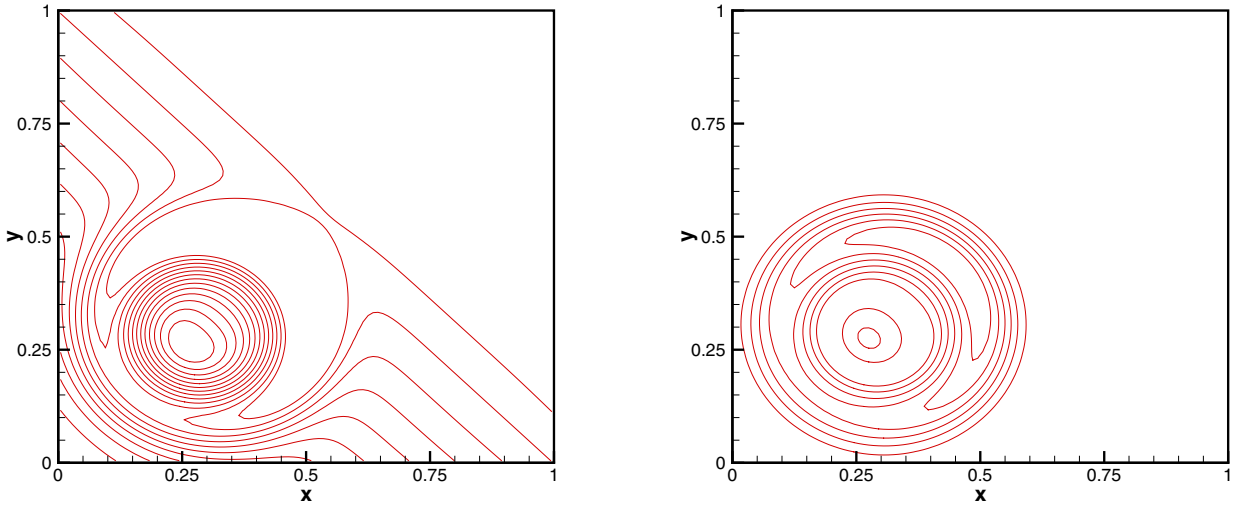

Fig. 8. Perturbation to the polytropic hydrostatic solution with $\eta = 0.1$ in Section 4.6. Contours of numerical results by non-well-balanced DG methods with 100×100 cells at $t = 0.15$. Left: twenty equally spaced contours between -0.03 and $+0.03$ of pressure perturbation. Right: twenty equally spaced contours between 0.01 and 0.12 of velocity $\left(\sqrt{u^2 + v^2}\right)$.

$$\begin{aligned} \rho_e(x,y) &= (T_e(x,y))^{\frac{1}{\gamma-1}}, \\ u_e(x,y) &= 0, \\ v_e(x,y) &= 0, \\ p_e(x,y) &= (T_e(x,y))^{\frac{\gamma}{\gamma-1}}, \end{aligned} \tag{38}$$

on a unit domain $[0, 1] \times [0, 1]$ with $T_e(x,y) = 1 - \frac{\gamma-1}{\gamma}\phi(x,y)$ and $\phi(x,y) = x + y$ as well as $\gamma = 1.4$.

Subsequently, we impose a perturbation to the initial pressure from the above isentropic hydrostatic solutions (38):

$$\begin{aligned} &\rho(x,y,0) = \rho_e(x,y) \\ &u(x,y,0) = 0, \\ &v(x,y,0) = 0, \\ &p(x,y,0) = p_e(x,y) + 0.1\exp\left(-100\rho_0 g((x-0.3)^2 + (y-0.3)^2))/p_0\right), \end{aligned}$$

with $g = 1$, $\rho_0 = 1.21$ and $p_0 = 1$. We show the numerical results with perturbation size $\eta = 0.1$ at $t = 0.15$ by both well-balanced and non-well-balanced DG methods in Figs. 7 and 8. It is evident that the numerical results by the well-balanced

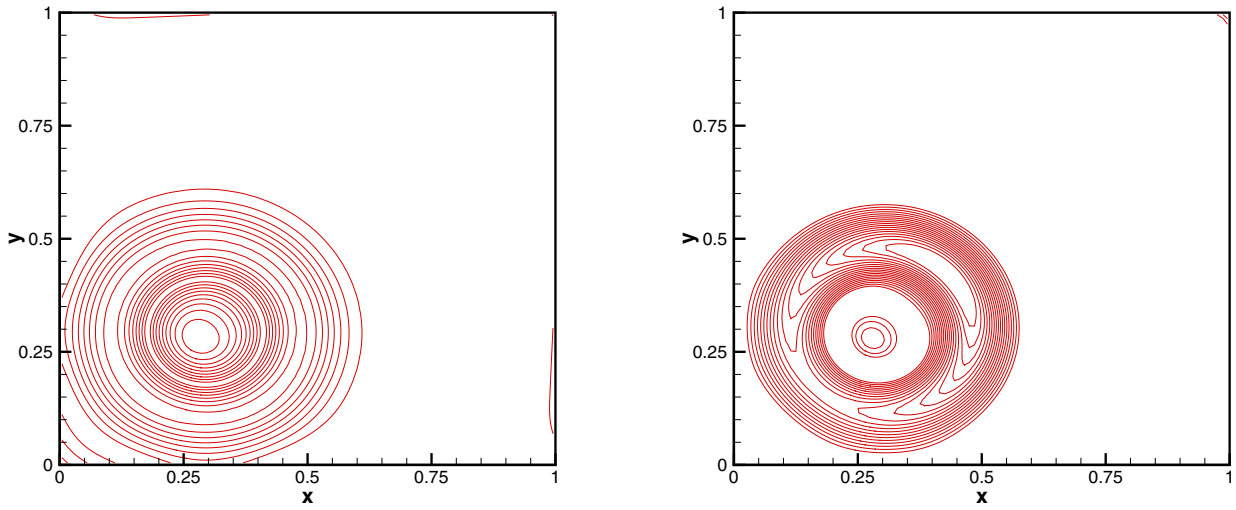

Fig. 9. Perturbation to the polytropic hydrostatic solution with $\eta = 0.001$ in Section 4.6. Contours of numerical results by well-balanced DG methods with 100×100 cells at $t = 0.15$. Left: twenty equally spaced contours between -0.00025 and $+0.00025$ of pressure perturbation. Right: twenty equally spaced contours between 0.0001 and 0.0014 of velocity $\left(\sqrt{u^2 + v^2}\right)$.

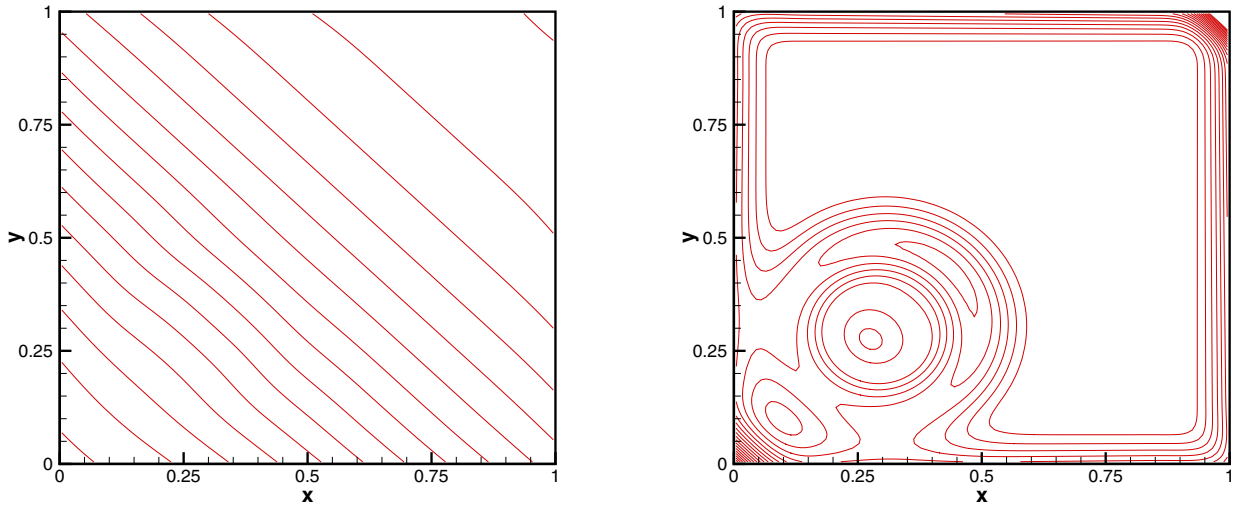

Fig. 10. Perturbation to the polytropic hydrostatic solution with $\eta = 0.001$ in Section 4.6. Contours of numerical results by non-well-balanced DG methods with 100×100 cells at $t = 0.15$. Left: twenty equally spaced contours between 0.006 and 0.025 of pressure perturbation. Right: twenty equally spaced contours between 0.0001 and 0.0014 of velocity $\left(\sqrt{u^2 + v^2}\right)$.

DG methods are with more resolution when compared with those by the non-well-balanced DG methods. Moreover, we reduce the size of the perturbation to $\eta = 0.001$ and repeat the simulation. The numerical results at $t = 0.15$ are shown in Figs. 9 and 10. Again, the well-balanced DG methods continue to produce numerical results with good resolution, while the non-well-balanced DG methods fail to capture the small perturbation thoroughly.

5. Concluding remarks

In this paper, we construct high order well-balanced DG methods for the Euler equations with isentropic equilibrium state under gravitational fields. In order to achieve the well-balanced property, special attention has been paid to the approximation of the source term as well as the construction of the numerical fluxes. Rigorous theoretical analysis indicates that the current methods maintain the well-balanced property. Moreover, extensive one- and two-dimensional numerical examples are also carried out to demonstrate the well-balanced property, high order accuracy, and good resolution of the proposed DG methods.

Acknowledgments

The research of the third author is supported by the Natural Science Foundation of PR China (11771228). The research of the fourth author is supported by the Natural Science Foundation of PR China (11321061, 11261160486, 91641107).

References

[1] P. Chandrashekar, C. Klingenberg, A second order well-balanced finite volume scheme for Euler equations with gravity, SIAM J. Sci. Comput. 37 (2015) 382–402.
[2] R. Käppeli, S. Mishra, Well-balanced schemes for the Euler equations with gravitation, J. Comput. Phys. 259 (2014) 199–219.
[3] Y. Xing, C.W. Shu, High order well-balanced WENO scheme for the gas dynamics equations under gravitational fields, J. Sci. Comput. 54 (2013) 645–662.
[4] C.T. Tian, K. Xu, K.L. Chan, L.C. Deng, A three-dimensional multidimensional gas-kinetic scheme for the Navier–Stokes equations under gravitational fields, J. Comput. Phys. 226 (2007) 2003–2027.
[5] K. Xu, J. Luo, S. Chen, A well-balanced kinetic scheme for gas dynamic equations under gravitational field, Adv. Appl. Math. Mech. 2 (2010) 200–210.
[6] J. Luo, K. Xu, N. Liu, A well-balanced symplecticity-preserving gas-kinetic scheme for hydrodynamic equations under gravitational field, SIAM J. Sci. Comput. 33 (2011) 2356–2381.
[7] M.M. Ginarda, M. Vázqueza, G. Houzeauxa, Local preconditioning and variational multiscale stabilization for Euler compressible steady flow, Comput. Methods Appl. Mech. Eng. 305 (2016) 468–500.
[8] R. Käppeli, S. Mishra, A well-balanced finite volume scheme for the Euler equations with gravitation. The exact preservation of hydrostatic equilibrium with arbitrary entropy stratification, Astron. Astrophys. 587 (2016) 1–16.
[9] N. Botta, R. Klein, S. Langenberg, S. Lützenkirchen, Well-balanced finite volume methods for nearly hydrostatic flows, J. Computat. Phys. 196 (2004) 539–565.
[10] Y.L. Xing, C.W. Shu, S. Noelle, On the advantage of well-balanced schemes for moving-water equilibria of the shallow water equations, J. Sci. Comput. 48 (2011) 339–349.
[11] J.M. Greenberg, A.Y. Leroux, A well-balanced scheme for the numerical processing of source terms in hyperbolic equations, SIAM J. Numer. Anal. 33 (1996) 1–16.
[12] J.M. Greenberg, A.Y. Leroux, R. Baraille, A. Noussair, Analysis and approximation of conservation laws with source terms, SIAM J. Numer. Anal. 34 (1997) 1980–2007.
[13] S. Noelle, Y.L. Xing, C.W. Shu, High-order well-balanced schemes, in: G. Puppo, G. Russo (Eds.), Numerical Methods for Balance Laws, Quaderni di Matematica, 2010.
[14] R.J. LeVeque, D.S. Bale, Wave propagation methods for conservation laws with source terms, in: Proceedings of the Seventh International Conference on Hyperbolic Problems, 1998, pp. 609–618.
[15] D. Ghosh, E.M. Constantinescu, Well-balanced, conservative finite difference algorithm for atmospheric flows, AIAA J. 54 (2016) 1370–1385.
[16] G. Li, Y. Xing, Well-balanced discontinuous Galerkin methods for the Euler equations under gravitational fields, J. Sci. Comput. 67 (2016) 493–513.
[17] G. Li, Y. Xing, High order finite volume WENO schemes for the Euler equations under gravitational fields, J. Comput. Phys. 316 (2016) 145–163.
[18] G. Li, Y. Xing, Well-balanced finite difference weighted essentially non-oscillatory schemes for the Euler equations with static gravitational fields, Comput. Math. Appl. https://doi.org/10.1016/j.camwa.2017.10.015.
[19] G. Li, Y.L. Xing, Well-balanced discontinuous Galerkin methods with hydrostatic reconstruction for the Euler equations with gravitation, J. Comput. Phys. 352 (2018) 445–462.
[20] A. Chertock, S. Cui, A. Kurganovz, S.N. Özcan, E. Tadmor, Well-balanced schemes for the Euler equations with gravitation: Conservative formulation using global fluxes, J. Comput. Phys. 358 (2018) 36–52.
[21] V. Desveaux, M. Zenk, C. Berthon, C. Klingenberg, A well-balanced scheme for the Euler equation with a gravitational potential, in: Finite Volumes for Complex Applications VII-Methods and Theoretical Aspects, in: Springer Proceedings in Mathematics & Statistics, 77, Springer, 2014, pp. 217–226.
[22] M. Zingale, L.J. Dursi, J. ZuHone, A.C. Calder, B. Fryxell, T. Plewa, J.W. Truran, A. Caceres, K. Olson, P.M. Ricker, K. Riley, R. Rosner, A. Siegel, F.X. Timmes, N. Vladimirova, Mapping initial hydrostatic models in Godunov codes, Astrophys. J. Suppl. Ser. 143 (2002) 539–565.
[23] V. Desveaux, M. Zenk, C. Berthon, C. Klingenberg, A well-balanced scheme to capture non-explicit steady states in the Euler equations with gravity, Int. J. Numer. Methods Fluids 81 (2016) 104–127.
[24] B. Cockburn, G. Karniadakis, C.W. Shu, The development of discontinuous Galerkin methods, in: B. Cockburn, G. Karniadakis, C.W. Shu (Eds.), Discontinuous Galerkin Methods: Theory, Computation and Applications, Lecture Notes in Computational Science and Engineering, Part I: Overview, 11, Springer, 2000, pp. 3–50.
[25] C.W. Shu, High order WENO and DG methods for time-dependent convection-dominated PDEs: a brief survey of several recent developments, J. Comput. Phys. 316 (2016) 598–613.
[26] B. Cockburn, C.W. Shu, Runge–utta discontinuous Galerkin methods for convection-dominated problems, J. Sci. Comput. 16 (2001) 173–261.
[27] B. Cockburn, F. Li, C.W. Shu, Locally divergence-free discontinuous Galerkin methods for the Maxwell equations, J. Comput. Phys. 194 (2004) 588–610.
[28] F. Li, C.W. Shu, Locally divergence-free discontinuous Galerkin methods for MHD equations, J. Sci. Comput. 22–23 (2005) 413–442.
[29] C.W. Shu, Total-variation-diminishing time discretizations, SIAM J. Sci. Stat. Comput. 9 (1988) 1073–1084.
[30] C.W. Shu, TVB uniformly high-order schemes for conservation laws, Math. Comput. 49 (1987) 105–121.
[31] B. Cockburn, C.W. Shu, The Runge–Kutta discontinuous Galerkin method for conservation laws v: multidimensional systems, J. Comput. Phys. 141 (1998) 199–224.